Numerical simulation of the Richtmyer-Meshkov instability in initially nonuniform flows and mixing with reshock

Jing-song Bai,[1,2] Bing Wang,[1] Tao Wang,[1] and Kun Liu[1]

[1]*Institute of Fluid Physics, China Academy of Engineering Physics, Mianyang, Sichuan, People's Republic of China*

[2]*National Key Laboratory of Shock Wave and Detonation Physics (LSD), Institute of Fluid Physics, China Academy of Engineering Physics, Mianyang, Sichuan, People's Republic of China*

(Received 14 September 2012; published 26 December 2012)

Based on previous instability experiments of the double mode perturbed interface in initially nonuniform flows, we numerically investigate the effect of the nonuniformity of flows on the evolution of instability in a nonlinear regime after reshock by adopting two different nonuniform coefficients ($\delta_1 = 0.6162$ and $\delta_2 = 0.4961$) in the Gaussian distribution of the initial nonuniform density. We obtain the evolution of the mixing zone width and vortex structure of the air-SF_6 interface and compare the circulation discrepancies of the nonuniform and uniform flows before and after reshock. These results indicate that the nonuniformity of the initial flow has great effect on the evolution of instability in the linear regime and the weak nonlinear regime prior to reshock. However, the mixing layer has little dependence on the nonuniformity of the initial flow in the nonlinear regime after reshock; namely, the effect of the nonuniformity is reduced significantly as the instability enters the strongly nonlinear regime after reshock. Although the growth rate of the perturbations has a significant increase, the characteristics of the flow like the mixing width, vorticity, and circulation are close to those of a uniform flow.

DOI: 10.1103/PhysRevE.86.066319 PACS number(s): 47.40.Nm, 47.20.Ma

The Richtmyer-Meshkov instability occurring at the corrugated interface between two fluids of different densities is of contemporary interest in many fields of research, among which are the inertial confinement fusion (ICF) [1], the fuel mixing in a Scramjet [2], and the explosion of supernovas [3]. When an incident shock proceeds into a perturbed interface, vorticity is deposited by the baroclinic torque vorticity production term $(\nabla\rho \times \nabla p)/\rho^2$.

Following the first interaction between the mixing layer and the shock, a transmitted shock proceeds into the second heavy fluid, this shock reflects from the end wall of the shock tube, and then it encounters the evolving layer again. After the process called reshock, a transmitted shock passes into the first fluid and a reflected rarefaction wave returns to the second fluid. The rarefaction wave repeats the process of the incident shock and again interacts with the evolving interface, producing a compression wave. The compression wave encounters the evolving mixing layer zone after reflecting from the end wall of the shock tube and then generates a shock returning to the second fluid. The compressibility and nonlinearity effects in wave-interface interactions significantly affect the growth rate, making analytical studies of the growth rate harder to conduct.

Numerous investigations focusing on the growth rate after reshocks have been presented. In 1960, Richtmyer [4] originally confirmed that the growth rate of the initially small perturbation amplitude in single-mode Richtmyer-Meshkov instability is linearized with time. Mikaelian [5] explored the growth rate of the interface by applying the potential flow model to growing perturbation to combine the initial and asymptotic stages, extending Richtmyer's linear impulsive theory. Zhang and Sohn [6] presented a derivation of the nonlinear theory of Richtmyer-Meshkov (RM) instability using a Padé approximation from early to later times. Recently, a number of studies have investigated the effects of the initial conditions on the growth rate. Thornber *et al.* [7] showed that the effects of the initial conditions will diminish after a few reshocks because of the change of the form of the perturbation power spectrum. Schilling *et al.* [8] used the ninth-order-weighted, essentially nonoscillatory shock-capturing method to investigate the late-time mechanism of reshock and mixing, presenting the density, vorticity, baroclinic vorticity production, and simulated density Schlieren fields first to describe the reshock process, and confirmed that the reflected rarefaction has an important role in breaking symmetry and approaching late-time statistical isotropy of the velocity field. Hill *et al.* [9] indicated that the reflected rarefaction drives the growth rate of the mixing layer more significantly than the reshock by examining the turbulent kinetic energy. Ukai *et al.* [10] investigated the effect of the initial conditions on the late-time growth by studying four different initial configurations of the interface numerically and found that growth rates after reshock have a little dependence on the initial interface geometry. Leinov *et al.* [11] showed that the growth rate after reshocks is independent of the initial amplitude by placing the rigid end wall at different distances from the initial contact interface in RM instability experiments.

In the literature published, the initial flows were confined to a uniform flow field. In 2010, we investigated the effects of the initially nonuniform flows on the evolution of the instability with the experiment and the numerical simulation of the double perturbed interface in nonuniform flows [12]. In addition, the initial density distribution of the nonuniform flows was determined quantitatively by the combination of numerical simulation and experimental phenomena and data, and then the effects of nonuniform flows on the evolution of the perturbation in RM instability was understood by recurring the whole experiment. This work is important for the setting of initial conditions and experimental data analysis in the experimental study of RM instability. This paper investigates the effects of the nonuniformity of the initial flows on the evolution of the mixing zone in RM instability under reshocks. Numerical simulation of RM instability for two initially nonuniform flows under shock and reshock is performed. The quantitative analysis of the mixing width, vorticity, and circulation demonstrates

the effects of the initial conditions on the interface instability. The evolution principle of interface instability in the strongly nonlinear regime after reshock in the nonuniform flows is obtained. These results are expected to shed new light on the turbulent mixing induced by RM instability.

This paper applies our large eddy simulation code MVFT (multiviscous flow and turbulent) to numerically simulate the multiviscosity fluid and turbulence. The code MVFT was used for the compressible large eddy simulation that was developed by Institute of Fluid Physics at the China Academy of Engineering Physics. MVFT can be used to simulate multicomponent flows, and compute shocks, contact discontinuities and material interfaces at high accuracy. It splits the flow into an inviscid flow and a viscous flow by using an operator splitting technique, where the former is computed by employing the piecewise parabolic method with a third-order Godunov scheme and the latter is calculated by utilizing a central difference scheme in conjunction with a second-order Runge-Kutta method.

MVFT applies based on the piecewise parabolic method [13] to interpolate physical quantities, the Vreman [14] subgrid eddy viscosity model to conduct large eddy simulation, and to solve the Navier-Stokes equations:

$$
\begin{aligned}
&\frac{\partial \bar{\rho}}{\partial t}+\frac{\partial \bar{\rho}\tilde{u}_j}{\partial x_j}=0\\
&\frac{\partial \bar{\rho}\tilde{u}_i}{\partial t}+\frac{\partial \bar{\rho}\tilde{u}_j\tilde{u}_i}{\partial x_j}+\frac{\partial \bar{p}}{\partial x_i}=\frac{\partial(\bar{\sigma}_{ij}+\tau_{ij})}{\partial x_j}\\
&\frac{\partial \bar{\rho}\bar{E}}{\partial t}+\frac{\partial(\bar{\rho}\tilde{u}_j\bar{E}+\bar{p}\tilde{u}_j)}{\partial x_j}=-\frac{\partial(\bar{q}_j+Q_j)}{\partial x_j}+\frac{\partial(\tilde{u}_i(\bar{\sigma}_{ij}+\tau_{ij}))}{\partial x_j}\\
&\frac{\partial \bar{Y}^{(s)}}{\partial t}+\tilde{u}_j\frac{\partial \bar{Y}^{(s)}}{\partial x_j}=\frac{\partial}{\partial x_j}\Big(\tilde{D}\frac{\partial \bar{Y}^{(s)}}{\partial x_j}\Big),\quad s=1,2,\ldots,N-1.
\end{aligned}
\tag{1}
$$

$\bar{\sigma}_{ij}=\mu_l[\partial\tilde{u}_i/\partial x_j+\partial\tilde{u}_j/\partial x_i-2/3\delta_{ij}(\partial\tilde{u}_k/\partial x_k)]$ is the viscous stress tensor, $\tau_{ij}=\rho(\overline{u_iu_j}-\bar{u}_i\bar{u}_j)$ is the subgrid scale (SGS) stress tensor, $\bar{q}_j+Q_j$ is the energy flux of unit time and space, $\bar{q}_j=-\lambda_l\partial\bar{T}/\partial x_j$, $Q_j=-\lambda_t\partial\bar{T}/\partial x_j$, $\lambda_l=\mu_l c_p/p_{r,l}$, $\lambda_t=\mu_t c_p/p_{r,t}$, $\tilde{D}=\bar{D}_l+D_t$, $S_{c,t}=\mu_t/D_t\bar{\rho}$, μ_l is the fluid viscosity, μ_t is the turbulent viscosity, $\bar{T}$ is the temperature, λ_l is the efficient heat-transfer coefficient, c_p is the specific heat of fluid, $p_{r,l}$ is the Prandtl number, $\bar{D}_l$ is the diffusion coefficient, and D_t is the turbulent diffusion coefficient. An operator splitting technique is used to decompose the physical problems into three subprocesses in MVFT, i.e., the computations of inviscid flux, viscous flux, and heat flux. For the inviscid flux, the three-dimensional problem can be simplified into three one-dimensional (1D) problems by the dimension splitting technique. For each 1D problem, we apply a two-step Lagrange-Remap algorithm to solve the equations and a time step calculation can be divided into four steps: (i) piecewise parabolic interpolation of physical quantities, (ii) solving Riemann problems approximately, (iii) evolution of Lagrange equations, and (iv) remapping the physical quantities to stationary Euler meshes. The governing equations, algorithms, numerical schemes, SGS turbulent model, etc., are presented in Ref. [15].

We also chose the air and SF_6 gases, the same as Ref [12], and hope the SF_6 gas constitutes the initial nonuniform flow field. The air-SF_6 interface for single-mode sinusoidal perturbation is such that the wavelength is $\lambda=0.05$ m, the wave number is $\omega=2\pi/\lambda$, the amplitude is $A=5.0\times10^{-3}$ m, and the perturbation function is $x=A\sin(\omega y)$. The incident shock wave Mach number is 1.25 in air. The initial structure diagram

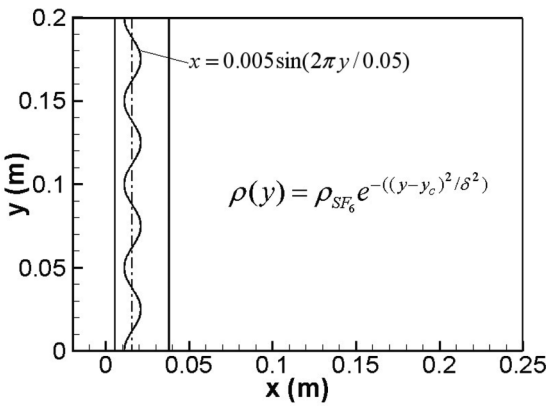

FIG. 1. Initial structure diagram in the shock tube.

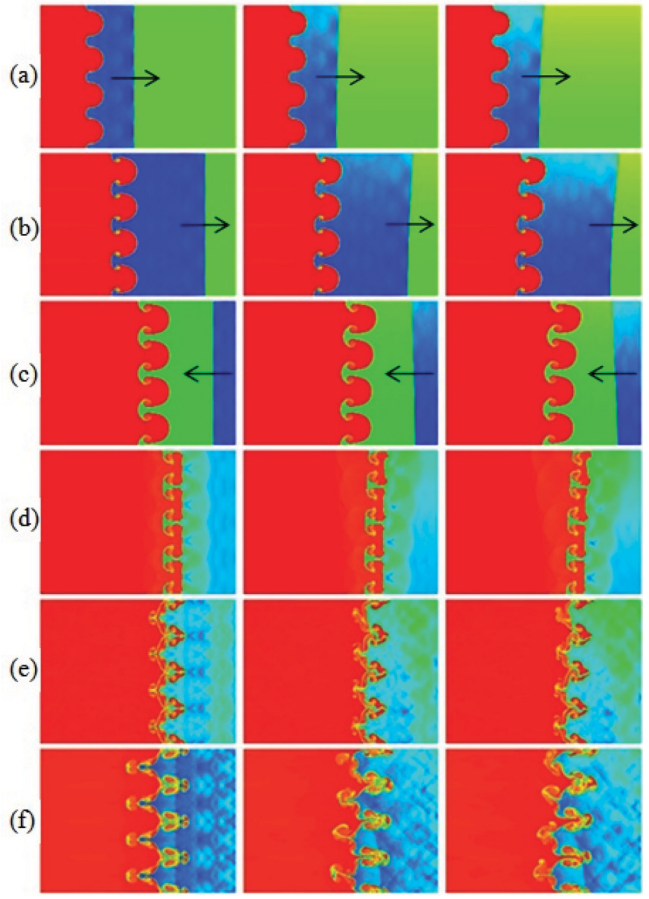

FIG. 2. (Color online) Density contour images of the numerical simulation result by MVFT at certain times: (a) 0.5 ms, (b) 1.0 ms, (c) 1.5 ms, (d) 2.0 ms, (e) 2.5 ms, and (f) 3.0 ms. Left column, uniform initial conditions; middle column, δ_1 nonuniform Gaussian function; and right column, δ_2 nonuniform Gaussian function. The small arrow denotes the direction of propagation of the shock wave fronts before reshock of the interface.

TABLE I. Properties of air and SF_6 gases.

Gases	Density (kg/m^3)	Specific heat ratio	Kinematic viscosity (10^{-6} m^2/s)	Prandtl number	Diffusion coefficient in air (cm^2/s)
Air	1.29	1.40	15.7	0.71	0.204
SF_6	5.34	1.09	2.47	0.90	0.097

is shown in Fig. 1, the initial shock front is located at $x = 5.56 \times 10^{-3}$ m, and the equilibrium position of perturbation is at $x = 0.016$ m.

In the simulation, we give two initial nonuniform flows for the SF_6 gas. The SF_6 gas densities in the lower part of shock tube are both ρ_{SF_6}, and the densities at the upper part of the shock tube are $0.9\rho_{SF_6}$ and $0.85\rho_{SF_6}$, respectively. The initial SF_6 gas density of the nonuniform flows is calculated by the Gaussian function,

$$\rho(y) = \rho_{SF_6} e^{-[(y-y_c)^2/\delta^2]}, \tag{2}$$

where $y_c = 0$ and the nonuniform coefficients are $\delta_1 = 0.6162$ m and $\delta_2 = 0.4961$ m. The less the nonuniform coefficient is, the stronger the nonuniformity of the flow is. The computational domain is [–0.02 m, 0.25 m] × [0.0 m, 0.2 m], and it is discretized into 540 × 400 grids with a rigid wall condition to the right boundary. Table I summarizes the properties of air and SF_6 gases in the present experiment at 1 atmospheric pressure and 20°C.

In order to analyze the results of the initial nonuniform flows with different Gaussian distributions, the simulation for the uniform flow is also performed. Figures 2–4 show the density, vortex, and volume of fraction of SF_6 gas contour images of the numerical simulation results by MVFT at a time of from 0.5 to 3.0 ms with 0.5-ms intervals. The left, middle, and right column images in Figs. 2–4 correspond with the uniform initial condition simulation results, the δ_1 nonuniform Gaussian function cases, and the δ_2 nonuniform Gaussian function cases, respectively. Figures 2–4 indicate qualitatively that the transmitted shock and the reflected shock can conserve the planarity, and after the interaction with shocks, the disturbed interface can also preserve good periodicity before and after reshock. The nonuniformity of the RM instability of the sinusoidal interface results from the density variances of the SF_6 gas in the nonuniform flows which make the transmitted and reflected shocks inclined. However, the simulation results show that there is a significant difference between the uniform and nonuniform flows before reshock, such as the results of $t = 0.5$,

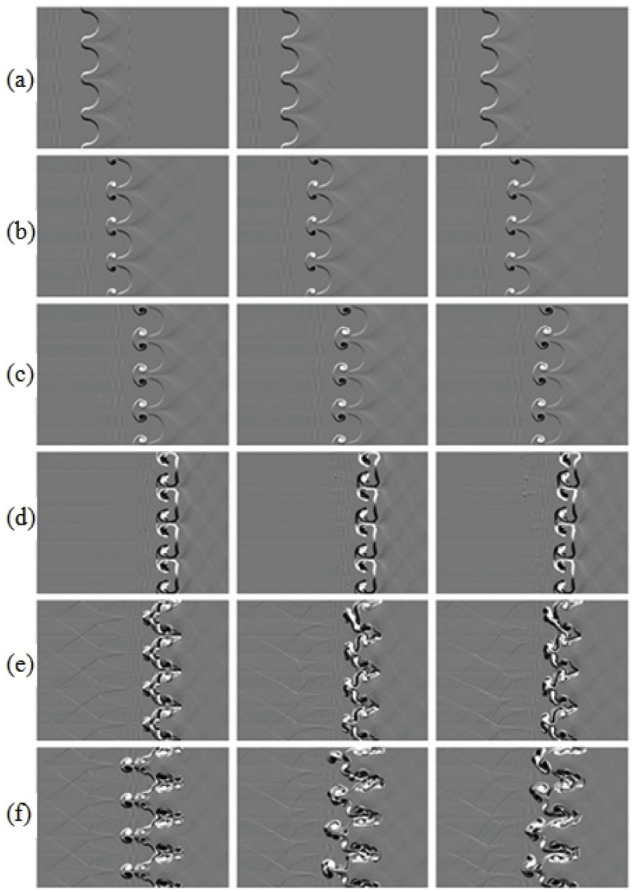

FIG. 3. Vortex contour images of the numerical simulation result by MVFT at certain times: (a) 0.5 ms, (b) 1.0 ms, (c) 1.5 ms, (d) 2.0 ms, (e) 2.5 ms, and (f) 3.0 ms. Left column, uniform initial conditions; middle column, δ_1 nonuniform Gaussian function; and right column, δ_2 nonuniform Gaussian function.

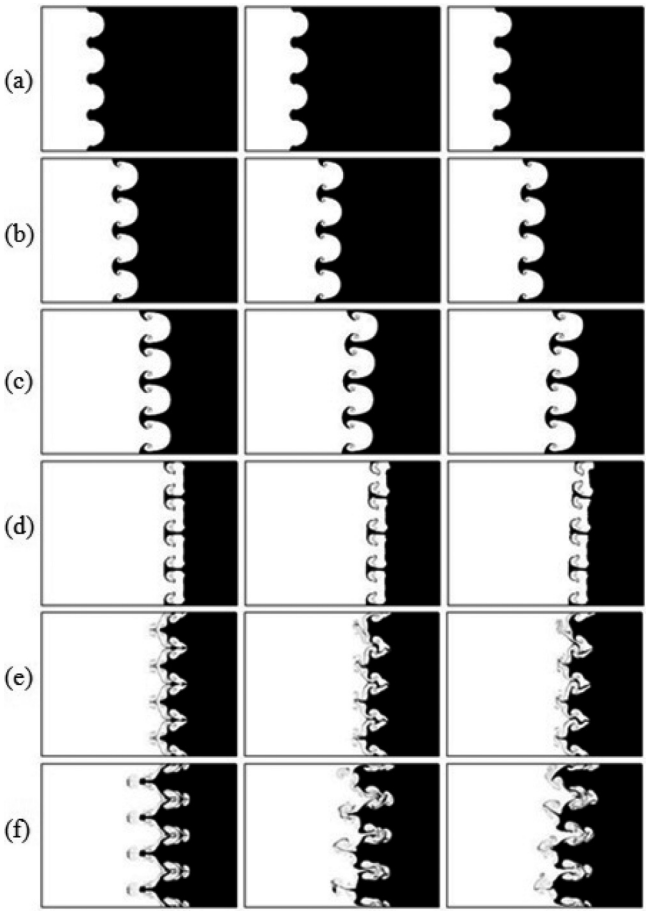

FIG. 4. Volume of fraction of SF_6 contour images of the numerical simulation result by MVFT at certain times: (a) 0.5 ms, (b) 1.0 ms, (c) 1.5 ms, (d) 2.0 ms, (e) 2.5 ms, and (f) 3.0 ms. Left column, uniform initial conditions; tmiddle column, δ_1 nonuniform Gaussian function; and right column, δ_2 nonuniform Gaussian function.

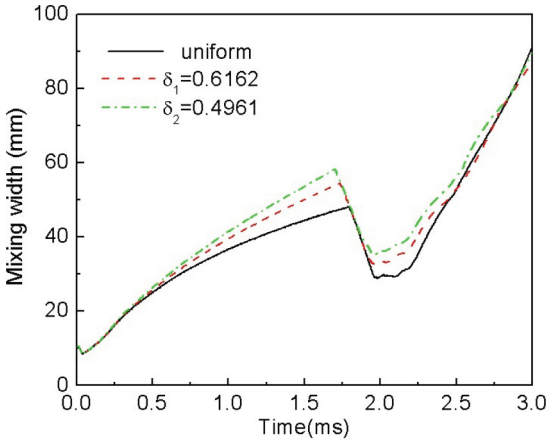

FIG. 5. (Color online) Mixing width history calculations of the initial uniform and nonuniform flows in RM instability.

1.0, and 1.5 ms, but the difference decreases in evidence after reshock, for instance, the results of $t = 2.0$, 2.5, and 3.0 ms.

To estimate the mixing width from the numerical simulations, we calculate in each abscissa x the transversal averaged volume fraction $\bar{Y}(x)$ and define the abscissa x between $\bar{Y}(x)$ 0.01 and 0.99 as the mixing zone width. Figure 5 shows the mixing width history calculations of the initial uniform and nonuniform flows in RM instability. Figure 5 points out that the growth rate of the mixing width for the initial nonuniform flows is greater than that of the uniform flow, and the less the nonuniform coefficient is, the higher the growth rate of the mixing width is, but the difference among the three different flow configurations diminishes after reshock. These results indicate that the evolution of the instability has great dependence on the nonuniformity of the initial flow in the linear and weakly nonlinear regime prior to reshock; however, the effect of the nonuniformity is reduced significantly with the instability entering the strongly nonlinear regime after reshock. Although the growth of the perturbation is enhanced, the amplitude of the perturbation is close to a uniform flow compared with the previous regime.

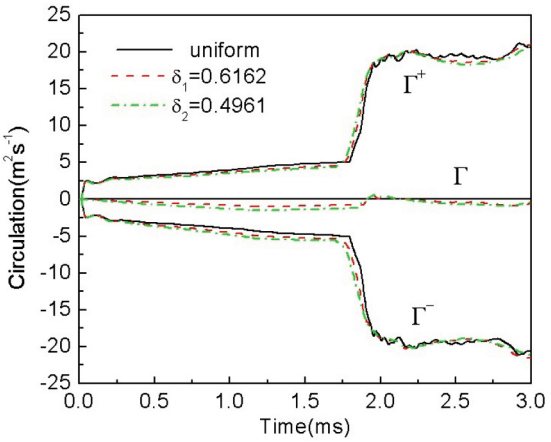

FIG. 6. (Color online) The positive circulation, the negative circulation, and the total circulation evolution over time of the flow field of the two elliptic gas cylinders.

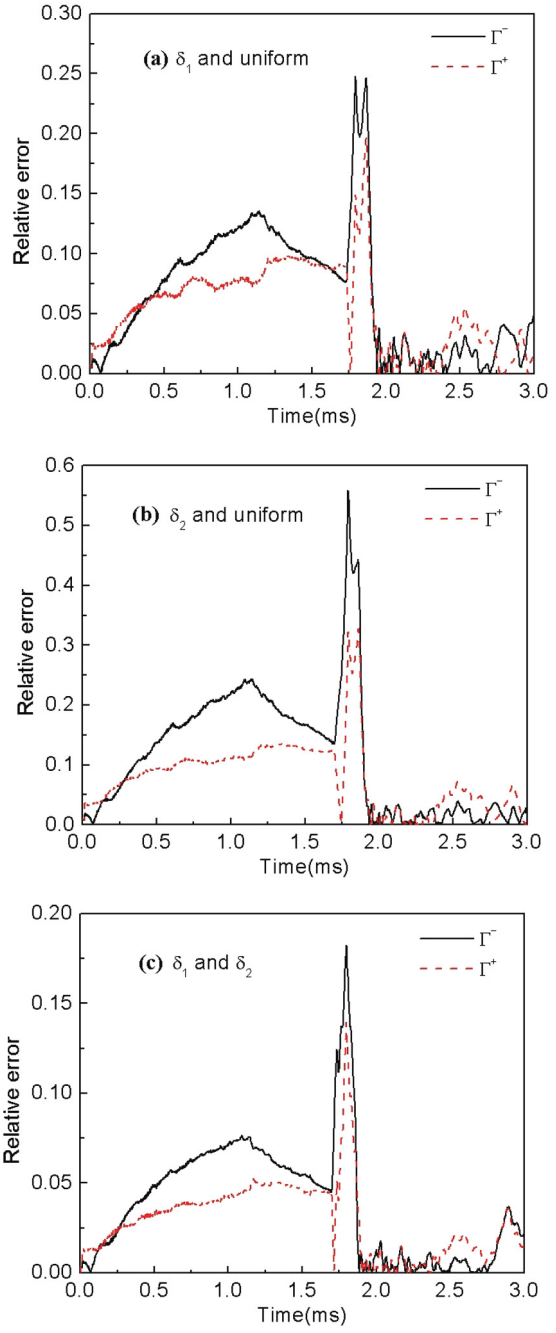

FIG. 7. (Color online) Relative error between the flow field in the positive and negative circulations, including the comparison between the nonuniform coefficients δ_1 and δ_2 with the uniform flow [panels (a) and (b)] and the nonuniform coefficient between the δ_1 and δ_2 [panel (c)]. The reshock times are 1.73, 1.70, and 1.70 ms, respectively, for the three graphs.

This evolution process of the mixing width is a macro description of numerical simulation to RM instability and mixing. To interpret the phenomena, the analysis of the underlying mechanism resulting in RM instability is required, namely, the analysis of the effects of the vorticity deposited by the baroclinic torque production term and the circulation in the mixing zone induced by RM instability. In the MVFT code, vorticity is determined by calculating the curl of the velocity

field. This relationship for the 2D flow is

$$\omega(x,y,t) = (\nabla \times \mathbf{V}) \cdot \mathbf{n} = \partial v/\partial x - \partial u/\partial y, \quad (3)$$

where $\mathbf{V}$ is the 2D velocity vector, and u and v are the x and y components of the velocity. Circulation is a measure of the average vorticity over an area A,

$$\Gamma(t) = \int_A \omega(x,y,t) dA. \quad (4)$$

Figure 6 shows the positive circulation Γ^+, the negative circulation Γ^- and the total circulation $\Gamma = \Gamma^+ + \Gamma^-$ evolution over time of the flow field. In Fig. 6, the results indicate that Γ^+ and Γ^- conserve the very good symmetry for the initial uniform flow, and the total circulation Γ is 0 all the time. For the initial nonuniform flows, Γ^+ and Γ^- no longer conserve symmetry due to the dissymmetry growth of the perturbation. And the total circulations of the flows Γ are nonzero. In order to further analyze the differences among three sets of curves in Fig. 6, more detailed comparisons should be made. The relative errors of the circulations (both positive Γ^+ and negative Γ^-) between the two initial nonuniform and the uniform flows are presented in the Figs. 7(a) and 7(b), respectively. Figure 7(a) shows the maximum differences of Γ^+ and Γ^- are 9.8% and 13.8%, respectively, before reshock; the maximum differences reach 19.7% and 24.8% in the transition regime; and the maximum departures are only 5.6% and 4.8% after reshock for the flow with the nonuniform coefficient δ_1. Corresponding to Fig. 7(a), Fig. 7(b) shows the maximum differences of Γ^+ and Γ^- are 13.6% and 24.5%, 32.7% and 55.7%, and 7.3% and 4.0% before reshock, in the transition regime, and after reshock, respectively, for the flow with the nonuniform coefficient δ_2. These results indicate that the differences between the nonuniform coefficients compared to the uniform flow exist prior to reshock and in the transition regime, and they diminish significantly after reshock with a mean value of 5% approximately. Because the circulation in the flow exists in the interface zone, it affects the evolution of the mixing zone directly. In addition, the difference between two initial nonuniform flows with nonuniform coefficients δ_1 and δ_2 is also exhibited in Fig. 7(c) which shows that the maximum differences of Γ^+ and Γ^- are 5.3% and 7.6% before reshock, 13.9% and 18.2% in the transition regime, and 3.6% and 3.7% after reshock, respectively.

In summary, we numerically simulate RM instability and mixing of the air-SF_6 interface with sinusoidal perturbation under shocks and reshocks by constructing two initial nonuniform density flows of the Gaussian distribution function with different coefficients of $\delta_1 = 0.6162$ and $\delta_2 = 0.4961$. The distinctions of the evolution and development of the mixing zone between nonuniform cases and uniform ones are analyzed. The results demonstrate that the evolution of the instability has a great dependence on the nonuniformity of the initial flow field in the linear regime and the weak nonlinear regime prior to reshock. Nevertheless, the effect of the nonuniformity is reduced significantly as the instability enters the strongly nonlinear regime after reshock. Although the growth of the perturbation is enhanced in this regime, the amplitude of the perturbation is close to that of a uniform flow compared with the previous regime. The reason for the abovementioned phenomena is presented with the quantitative analysis of the circulation. In addition, the comparisons of the computational results between two initial nonuniform flows are shown. This paper further demonstrates that the effects of the initial conditions of flows on the macro scale characteristics are weakened gradually in the later time of RM instability. Naturally, we speculate that the flow field will completely forget the effects of the initial conditions in the fully developed regime, which can become turbulent.

ACKNOWLEDGMENTS

This work was sponsored by the National Science Foundation of China under Grants No. 11072228 and No. 11202195 and the Science Foundation of the China Academy of Engineering Physics under Grants No. 2011B0202005 and No. 2011A0201002

[1] J. D. Lindl, R. L. McCropy, and E. M. Campbell, Phys. Today **45**, 32 (1992).
[2] J. Yang, T. Kubota, and E. E. Zukoski, AIAA J. **31**, 5 (1993).
[3] D. Arnett, Astrophys. J., Suppl. Ser. **127**, 213 (2000).
[4] R. D. Richtmyer, Commun. Pure Appl. Math. **13**, 297 (1960).
[5] K. O. Mikaelian, Phys. Rev. E **67**, 026319 (2003).
[6] Qiang Zhang and Sung-Ik Sohn, Z. Angew. Math. Phys. **50**, 1 (1999).
[7] B. Thornber, D. Drikakis, D. L. Youngs, and R. J. R. Williams, Phys. Fluids **23**, 095107 (2011).
[8] Oleg Schilling, Marco Latini, and Wai Sun Don, Phys. Rev. E **76**, 026319 (2007).
[9] D. J. Hill, C. Pantano, and D. I. Pullin, J. Fluid Mech. **557**, 29 (2006)
[10] S. Ukai, K. Balakrishnan, and S. Menon, Shock Waves **21**, 533(2011).
[11] E. Leinov, O. Sadot, A. Formoza, G. Malamud, Y. Elbaz, L. A. Levin, G. Ben-Dor, and D. Shvarts, Phys. Scr., T **132**, 014014 (2008).
[12] J. S. Bai, J. H. Liu, T. Wang, L. Y. Zou, P. Li, and D. W. Tan, Phys. Rev. E **81**, 056302 (2010).
[13] P. Colella and P. R. Woodward, J. Comput. Phys. **54**, 174 (1984).
[14] W. Vreman, Phys. Fluids **16**, 3670(2004).
[15] J. S. Bai, L. Y. Zou, T. Wang, K. Liu, W. B. Huang, J. H. Liu, P. Li, D. W. Tan, and C. L. Liu, Phys. Rev. E **82**, 056318 (2010).